Ladder Dyson-Schwinger calculation of the anomalous γ-3π form factor

Stephen R. Cotanch* and Pieter Maris†
Department of Physics, North Carolina State University, Raleigh, North Carolina 27695-8202, USA
(Received 4 June 2003; published 29 August 2003)

The anomalous processes $\gamma \to 3\pi$ and $\gamma\pi \to \pi\pi$ are investigated within the Dyson-Schwinger framework using the rainbow-ladder approximation. Calculations reveal that a complete set of ladder diagrams beyond the impulse approximation are necessary to reproduce the fundamental low-energy theorem for the anomalous form factor. Higher momentum calculations also agree with the limited form factor data and exhibit the same resonance behavior as the phenomenological vector meson dominance model.

DOI: 10.1103/PhysRevD.68.036006 PACS number(s): 11.10.St, 11.30.Rd, 11.40.Ha, 12.38.Lg

I. INTRODUCTION

Anomalies, in particular the anomalous nonconservation of the axial vector current, are a consequence of renormalization and are thus potentially present in all gauge theories. In fact a conserved axial vector current is incompatible with electromagnetic gauge invariance since radiative corrections lead to a nonzero current divergence. The quintessential example is the $\pi^0 \to \gamma\gamma$ decay, which, in the chiral limit, would be forbidden if the axial vector current was conserved. However, the form factor for this process, $F^{2\gamma}(Q^2)$, is nonzero and in the combined chiral and zero-momentum limit it is given by $F^{2\gamma}(Q^2) \to \hat{F}^{2\gamma}(0) = e^2/(4\pi^2 \hat{f}_\pi) = \alpha/(\pi \hat{f}_\pi)$ [1,2], where e is the proton charge, α is the fine structure constant and $\hat{f}_\pi$ is the pion decay constant in the chiral limit.

This work addresses another anomalous process, $\gamma \to \pi^+\pi^0\pi^-$, which also should, but does not, vanish in the combined chiral and soft momentum limits. The form factor for this, and the crossing related process $\gamma\pi \to \pi\pi$, is denoted by $F^{3\pi}(s,t,u)$, where $s = -(P_3+P_4)^2$, $t = -(P_2+P_4)^2$, and $u = -(P_2+P_3)^2$, with P_i the pion momenta. In the chiral limit, and for zero four-momenta, Refs. [3–5] proved $\hat{F}^{3\pi}(0,0,0) = \hat{F}^{2\gamma}/(e\hat{f}_\pi^2) = e/(4\pi^2 \hat{f}_\pi^3)$.

Several issues, both experimental and theoretical, motivate this investigation. Experimentally, only limited low momentum information about $F^{3\pi}$ is available from Primakov production using the $\pi A \to \pi\pi A$ reaction [6] and, for timelike photons, from $e^+e^- \to 3\pi$ measurements [7–9]. However, measurements to determine the form factor for the process $\gamma\pi \to \pi\pi$ are now underway at JLab [10]. New results for the form factor $F^{3\pi}$ in the range $0.27\ \mathrm{GeV}^2 < s < 0.72\ \mathrm{GeV}^2$ are expected to be released in the near future [11].

Theoretically, there are published analyses [12–14] based on the set of Dyson-Schwinger equations (DSEs) in the rainbow-ladder truncation. These pioneering studies evaluated diagrams in the generalized impulse approximation (GIA). However, it is necessary to go beyond the impulse approximation in order to correctly describe π-π scattering [15,16]: consistency requires inclusion of all planar diagrams ignoring gluon self-interactions (triple and quartic gluon vertices). In the current study we apply the same scheme to γ-3π processes and elucidate that the rainbow-ladder truncation in combination with the GIA is insufficient for a realistic description.

The structure of this paper spans six sections. In the next section the DSE formalism for mesons is applied to evaluate $F^{3\pi}$. Our numerical results for the form factor for symmetric pion momenta are presented in Sec. III and the low-energy theorem is reproduced. In Sec. IV we compare our results with meson exchange models for more general pion momenta. Finally, we confront the limited data in Sec. V and then summarize our conclusions in the final section.

II. MESON INTERACTIONS IN THE DYSON-SCHWINGER APPROACH

A. Dyson-Schwinger equations

Here we briefly summarize the DSE formalism applied to mesons. For more complete details consult Refs. [17–20]. Working in Euclidean space, with metric $\{\gamma_\mu, \gamma_\nu\} = 2\delta_{\mu\nu}$, $\gamma_\mu^\dagger = \gamma_\mu$ and $a \cdot b = a_i b_i \equiv \Sigma_{i=1}^4 a_i b_i$, the DSE for the renormalized quark propagator having four-momentum p is

$$S(p)^{-1} = iZ_2 \not{p} + Z_4 m_q(\mu) + Z_1 \int_q^\Lambda g^2 D_{\mu\nu}(k) \frac{\lambda^\alpha}{2} \gamma_\mu S(q) \Gamma_\nu^\alpha(q,p). \quad (1)$$

Here $\alpha = 1 \ldots 8$ is the color index, $D_{\mu\nu}(k)$ the dressed-gluon propagator and $\Gamma_\nu^\alpha(q,p)$ the dressed-quark-gluon vertex. The symbol $\int_q^\Lambda$ represents $\int_q^\Lambda [d^4k/(2\pi)^4]$ with $k = p - q$. Equation (1) has the general solution $S(p)^{-1} = i\not{p} A(p^2) + B(p^2)$ which is renormalized at spacelike μ^2 so that $A(\mu^2) = 1$ and $B(\mu^2) = m_q(\mu)$ with $m_q(\mu)$ being the current quark mass.

Mesons are modeled as $q^a \bar{q}^b$ bound states governed by the Bethe-Salpeter amplitude (BSA), Γ_H, which is a solution of the homogeneous Bethe-Salpeter equation (BSE). For quark flavors a, b and incoming, outgoing momenta $p_+ = p + P/2$, $p_- = p - P/2$, the BSE is

$$\Gamma_H^{a\bar{b}}(p_+, p_-) = \int_q^\Lambda K(p,q;P) S^a(q_+) \Gamma_H^{a\bar{b}}(q_+, q_-) S^b(q_-). \quad (2)$$

*Email address: cotanch@ncsu.edu
†Email address: pmaris@unity.ncsu.edu

The momenta $q_\pm$ are similarly defined. The renormalized, amputated $q\bar{q}$ scattering kernel, K, is irreducible with respect to a pair of $q\bar{q}$ lines. Equation (2) only admits solutions for discrete values of $P^2=-m_H^2$, where m_H is the meson mass. Imposing the canonical normalization condition for $q\bar{q}$ bound states then uniquely determines Γ_H. For pseudoscalar bound states the most general decomposition for $\Gamma_{PS}\equiv\Gamma_H^{a\bar{b}}$ is [21,22]

$$\Gamma_{PS}(q_+,q_-)=\gamma_5[iE(q^2,q\cdot P)+\not{P}F(q^2,q\cdot P) +\not{q}G(q^2,q\cdot P)+\sigma_{\mu\nu}P^\mu q^\nu H(q^2,q\cdot P)], \tag{3}$$

where the amplitudes E, F, G and H are Lorentz scalar functions of q^2 and $q\cdot P$. The odd C parity of the neutral pion requires that the amplitude G be odd in $q\cdot P$, while the others are even.

B. Rainbow-ladder truncation

The central approximation in this work is the rainbow-ladder truncation for the set of DSEs. For the quark DSE, Eq. (1), the rainbow truncation is

$$Z_1 g^2 D_{\mu\nu}(k)\Gamma^\alpha_\nu(q,p)\to\mathcal{G}(k^2)D^{\rm free}_{\mu\nu}(k)\gamma_\nu\frac{\lambda^\alpha}{2}, \tag{4}$$

where $D^{\rm free}_{\mu\nu}(k=p-q)$ is the free gluon propagator in the Landau gauge and $\mathcal{G}(k^2)$ is an effective $\bar{q}q$ interaction that reduces to the perturbative QCD running coupling in the ultraviolet region. For the BSE, Eq. (2), the ladder truncation is

$$K(p,q;P)\to-\mathcal{G}(k^2)D^{\rm free}_{\mu\nu}(k)\frac{\lambda^\alpha}{2}\gamma_\mu\frac{\lambda^\alpha}{2}\gamma_\nu. \tag{5}$$

These two truncations, in tandem, yield vector and axial vector vertices satisfying their respective Ward-Takahashi identities. This ensures chiral symmetry is respected with the pion being a massless Goldstone boson in the chiral limit [22–25]. Further, a conserved electromagnetic current is also obtained if the GIA is used to calculate electromagnetic form factors [26,27].

C. Amplitude for γ-3π processes

The above formalism is now applied to the $\gamma\to3\pi$ process to compute the anomalous amplitude, $A^{3\pi}$, and the corresponding form factor, $F^{3\pi}$. For simplicity, let us first consider one of the configurations that contribute to this process, depicted in the GIA in Fig. 1.

The quark lines in this figure represent dressed quark propagators, obtained as solutions of their DSE. The pion BSAs are solutions of the homogeneous BSE, and also the quark-photon vertex is dressed.

The Lorentz structure for this diagram is

$$a_\mu(P_2,P_3,P_4)=-i\epsilon_{\mu\nu\rho\sigma}P_2^\nu P_3^\rho P_4^\sigma f(s,t,u), \tag{6}$$

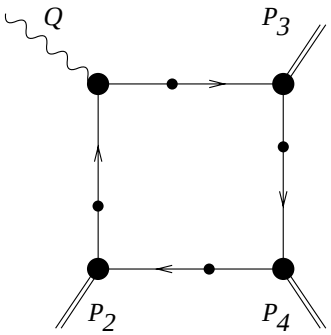

FIG. 1. The generic GIA diagram for γ-3π processes. All external momenta flow inward. The photon and three pions have momenta Q and P_i, $i=2,3,4$, respectively.

where $f(s,t,u)$ is a Lorentz scalar function of the Mandelstam variables $s=-(Q+P_2)^2$, $t=-(Q+P_3)^2$, $u=-(Q+P_4)^2$. All three pions are on-shell, $P_i^2=m_\pi^2$. The photon momentum is $Q=-(P_2+P_3+P_4)$ and Q^2 is related to the Mandelstam variables via

$$s+t+u=3m_\pi^2-Q^2. \tag{7}$$

The total $\gamma\to3\pi$ amplitude is obtained by summing over all six permutations of the three pions with the appropriate charge factors. It has the same Lorentz structure as Eq. (6), and can be written as

$$A^{3\pi}_\mu(P_2,P_3,P_4)=-i\epsilon_{\mu\nu\rho\sigma}P_2^\nu P_3^\rho P_4^\sigma F^{3\pi}(s,t,u). \tag{8}$$

In the isospin limit (equal masses for up and down quarks and ignoring electromagnetic corrections) all six configurations can be related through symmetry operations, which yields

$$F^{3\pi}(s,t,u)=\frac{e}{3}[f(s,t,u)+f(u,s,t)+f(t,u,s)]. \tag{9}$$

The process $\gamma\pi\to\pi\pi$ is described by the same form factor: the only difference is in the kinematical variables. For physical three-pion production, all three Mandelstam variables s, t and u must be above the threshold value $4m_\pi^2$. For $\gamma\pi\to\pi\pi$, the kinematics are different: $s>4m_\pi^2$ but $t,u<0$.

D. Corrections to the GIA

Although the GIA is consistent with current conservation for three-body processes such as electromagnetic form factors, it is insufficient, as demonstrated in detail in the next section, for four-body amplitudes such as π-π scattering and $F^{3\pi}$. It was previously noted [12] that if the Ball-Chiu [BC] ansatz [28] is used for the quark-photon vertex in combination with

$$\Gamma_{PS}=\frac{i\gamma_5}{f_\pi}B(q^2), \tag{10}$$

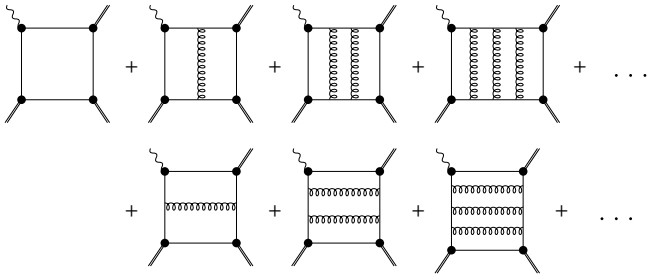

FIG. 2. Gluon exchange diagrams needed to correctly describe γ-3π processes in the rainbow-ladder truncation of the set of DSEs.

the GIA does reproduce the low-energy theorem[1]

$$\hat{F}^{3\pi}(0,0,0)=\frac{e}{4\pi^2\hat{f}_\pi^3}\approx 10.5\ \mathrm{GeV}^{-3}, \tag{11}$$

independent of model details for the scalar part of the quark self-energy, $B(q^2)$. However, this result is lost when the complete pion BSA [see Eq. (3)] is used.

A consistent treatment requires multiple *s*, *t* and *u*-channel gluon exchange, as depicted in Fig. 2 for one of the six configurations. This truncation scheme is equivalent to summing all planar diagrams ignoring gluon self-interactions (triple and quartic gluon vertices). The summation of the infinite set of ladder diagrams entails solving an inhomogeneous BSE of the type

$$G(p,P_i,P_j)=G_0(p,P_i,P_j)+\int_q^\Lambda \mathcal{G}(k^2)D^{\mathrm{free}}_{\mu\nu}(k)\frac{\lambda^\alpha}{2}\gamma_\mu S(q_+)$$
$$\times G(q,P_i,P_j)S(q_-)\frac{\lambda^\alpha}{2}\gamma_\nu, \tag{12}$$

where now $q_+=q+P_i$, $q_-=q-P_j$ and $G_0(p,P_i,P_j)$ is an inhomogeneous term of the form $\Gamma_\pi(p_+,p)S(p)\Gamma_\pi(p,p_-)$. For example, for the *s*-channel gluon exchange diagrams in Fig. 2 with $i=4$ and $j=3$

$$G_0(p,P_4,P_3)=\Gamma_\pi(p+P_4,p)S(p)\Gamma_\pi(p,p-P_3). \tag{13}$$

The corresponding amplitude for the sum of the GIA and the *s*-channel gluon exchange diagrams is (recall, momentum conservation dictates $P_2=-Q-P_3-P_4$)

$$a_\mu(P_2,P_3,P_4)=N_c\int_q^\Lambda \mathrm{Tr}[S(k+P_4)G(k,P_4,P_3)S(k-P_3)$$
$$\times\Gamma^\gamma_\mu(k-P_3,k-Q-P_3)S(k-Q-P_3)$$
$$\times\Gamma_\pi(k-Q-P_3,k+P_4)]. \tag{14}$$

[1]Note that the pion decay constant depends on the current quark mass: the chiral limit value is a few percent smaller than the physical value, $f_\pi=92.4$ MeV. In the model used here $\hat{f}_\pi=90$ MeV.

TABLE I. Selection of calculated and measured meson masses and coupling constants.

	Experiment [34] (estimates)	Calculated († fitted)
$m_{u=d}^{\mu=1\ \mathrm{GeV}}$	5–10 MeV	5.5 MeV
$-\langle qq\rangle_\mu^0$	$(236\ \mathrm{MeV})^3$	$(241\ \mathrm{MeV}^\dagger)^3$
m_π	138.5 MeV	$138^\dagger$ MeV
f_π	92.4 MeV	$92.5^\dagger$ MeV
m_ρ	771 MeV	742 MeV
g_ρ	5.01	5.07
$g_{\rho\pi\pi}$	6.02	5.14
m_ω	783 MeV	742 MeV
g_ω	17.06	15.2
m_σ	400∼1200 MeV	670 MeV

This treatment of the ladder diagrams is identical to the calculation reported for π-π scattering [16].

III. NUMERICAL RESULTS FOR SYMMETRIC PION MOMENTA

In contrast to DSE calculations for three-body processes, a significant computational effort is now necessary since *G* is a function of three independent variables: p^2, $p\cdot P_i$ and $p\cdot P_j$, for fixed P_i and P_j. Discretizing these variables on a three-dimensional grid, iteration is utilized starting with G_0. In the absence of singularities, convergence requires from 20 to 30 iterations. Close to a pole from an intermediate meson bound state, the number of required iterations increases dramatically. Typically, per fixed set of external variables (Q^2, *s*, *t* and *u*) away from intermediate meson poles, of order 20 CPU hours are needed to compute the form factor to an estimated precision of 2%. Our codes run on a parallel supercomputer (IBM SP) using 16 to 256 processors. Taking symmetric pion momenta reduces the necessary computer time by at least a factor of three.

A. Model parameters

The model interaction and parameters developed in Ref. [29] for the masses and decay constants of the light pseudoscalar and vector mesons are used for our numerical analysis. The effective $\bar{q}q$ interaction is

$$\frac{\mathcal{G}(k^2)}{k^2}=\frac{4\pi^2 D k^2}{\omega^6}\,\mathrm{e}^{-k^2/\omega^2}+\frac{4\pi^2\gamma_m\mathcal{F}(k^2)}{\frac{1}{2}\ln[\tau+(1+k^2/\Lambda_{\mathrm{QCD}}^2)^2]}, \tag{15}$$

with $\gamma_m=12/(33-2N_f)$, $N_f=4$, $\Lambda_{\mathrm{QCD}}=0.234$ GeV, $\tau=\mathrm{e}^2-1$, $\mathcal{F}(s)=[1-\exp(-s/4m_t^2)]/s$ and $m_t=0.5$ GeV. The renormalization scale, $\mu=19$ GeV, is within the perturbative domain [22,29]. The degenerate u/d quark mass, $m_{u=d}^{\mu=1\ \mathrm{GeV}}=5.5$ MeV, and remaining parameters, $\omega=0.4$ GeV, $D=0.93\ \mathrm{GeV}^2$, were determined by fitting m_π, f_π and the chiral condensate. Table I summarizes fitted, π, and pre-

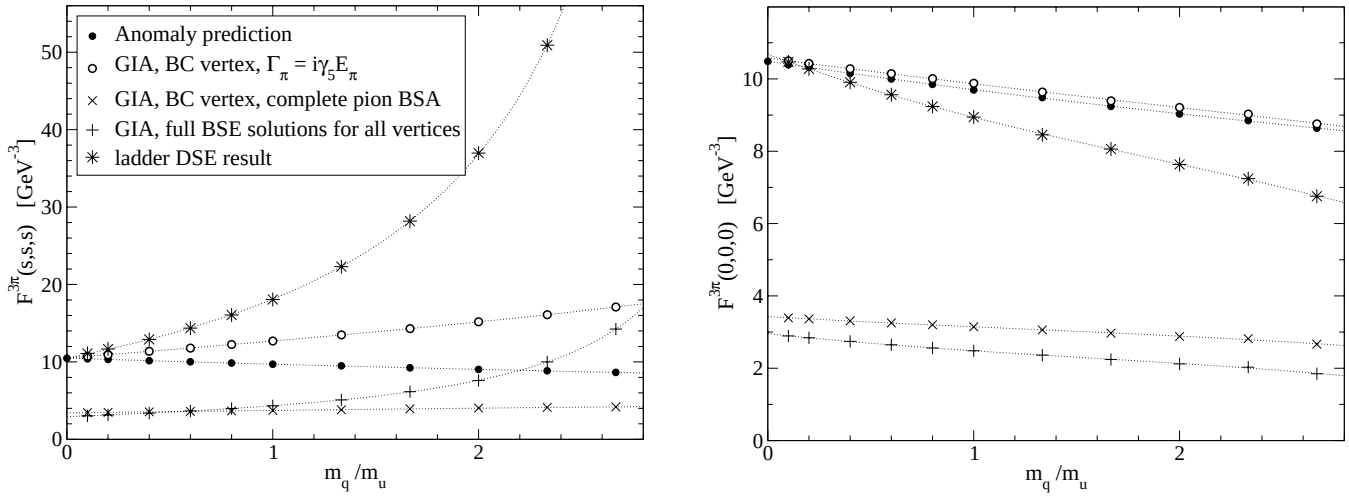

FIG. 3. Numerical results for the symmetric form factor $F^{3\pi}(4m_\pi^2,4m_\pi^2,4m_\pi^2)$ (left) and $F^{3\pi}(0,0,0)$ (right) as a function of the current quark mass m_q divided by the model up/down quark mass. The curves are fits to our numerical results (represented by the symbols) to guide the eye.

dicted, ρ and ω, masses which are in good agreement with observation [29]. The model's predictions are also in very good agreement with the most recent JLab data [30] for the $\pi^\pm$ form factor [27], $F_\pi(Q^2)$, and various other pion, ρ and ω observables [20,31,32], some of which are listed in Table I as well. In addition to a light pseudoscalar and vector meson, this model also exhibits a light scalar meson, putatively identified as the σ meson [16,33].

B. Quark mass dependence of $F^{3\pi}$

For symmetric pion momenta, $s=t=u$, Eq. (9) simplifies to

$$F^{3\pi}(s,s,s)=ef(s,s,s). \tag{16}$$

Since this reduces the necessary computer time significantly, we use this case to demonstrate that our scheme is in agreement with the low-energy theorem.

Note that the low-energy prediction, Eq. (11), corresponds to threshold production for three massless pions by an on-shell photon. However, for physical pions, the threshold for three-pion production is $s=t=u=4m_\pi^2$. On the other hand, for equal pion momenta, Eq. (7) reduces to $Q^2=3(m_\pi^2-s)$. Thus it is impossible to have on-shell photons ($Q^2=0$) producing three physical pions. Here we consider two limits, namely, threshold for three-pion production by timelike photons, $F^{3\pi}(4m_\pi^2,4m_\pi^2,4m_\pi^2)$ with $Q^2=-9m_\pi^2$, and $F^{3\pi}(0,0,0)$ with spacelike photon momenta $Q^2=3m_\pi^2$. In the chiral limit, both should approach $\hat{F}^{3\pi}(0,0,0)$. Our ladder DSE result for $F^{3\pi}$ is presented in Fig. 3, together with results obtained using the GIA in combination with different approximations for the vertices. There is a small dependence of the anomaly prediction on the current quark mass due to the fact that f_π depends on this mass. To avoid confusion with Eq. (11), we denote the (mass-dependent) anomaly prediction by

$$F^{3\pi}_{\text{anomaly}}(0,0,0)=\frac{e}{4\pi^2 f_\pi^3}. \tag{17}$$

For the physical current quark mass $f_\pi=92.4$ MeV and $F^{3\pi}_{\text{anomaly}}(0,0,0)=9.72\ \text{GeV}^{-3}$.

Our ladder DSE approach does indeed reproduce the correct result in the chiral limit. The strong dependence of the form factor at threshold, $F^{3\pi}(4m_\pi^2,4m_\pi^2,4m_\pi^2)$ with $Q^2=-9m_\pi^2$, is related to the ω pole in the quark-photon vertex at timelike photon momentum $Q^2=-m_\omega^2$. The form factor $F^{3\pi}(0,0,0)$ with spacelike $Q^2=3m_\pi^2$ is far less dependent on the quark mass. For on-shell photons, $Q^2=0$, $F^{3\pi}(m_\pi^2,m_\pi^2,m_\pi^2)$ is essentially independent of the current quark (and pion) mass.

The combination of GIA, BC ansatz for the quark-photon vertex and a purely pseudoscalar BSA also reproduces the correct chiral limit. However, the functional behavior approaching the chiral limit value is quite different from our scheme. This difference is predominantly due to the lack of intermediate meson states, in particular the ω, which is not incorporated in the BC ansatz. We address the importance of intermediate meson states in Sec. IV. In Fig. 3 also note that the GIA with the BC ansatz and full pion BSA including the pseudovector components F and G [see Eq. (3)], does not produce the correct chiral limit. Similarly, the GIA, with complete ladder BSE solutions for all vertices but without the additional ladder diagrams (see Fig. 2), does not yield the anomaly prediction.

C. Dependence on the photon momentum

The dependence of the form factor on the photon momentum is shown in Fig. 4 for both timelike and spacelike Q^2, using the model quark mass corresponding to physical pions. Again, all three on-shell pions have the same energy, $s=t=u=m_\pi^2-Q^2/3$, and the threshold for three-pion production is $Q^2=-9m_\pi^2\approx-0.172\ \text{GeV}^2$.

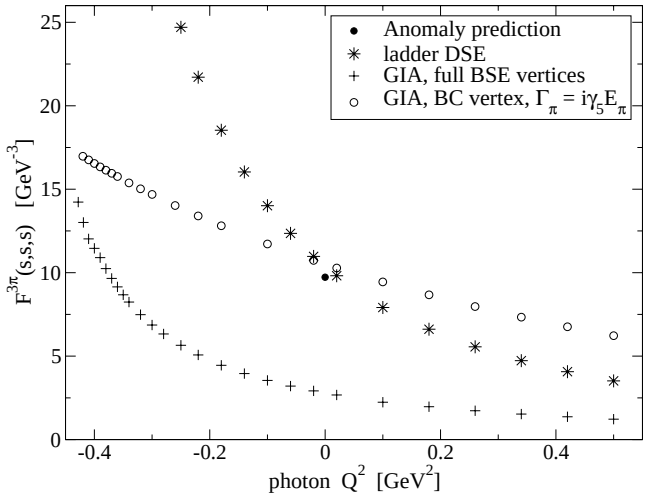

FIG. 4. Numerical results for the symmetric form factor $F^{3\pi}(s,s,s)$ as a function of Q^2.

Our result is in good agreement with the chiral anomaly prediction, as is the combination of the GIA and the BC ansatz for the quark-photon vertex using a purely pseudoscalar BSA. Now the difference between the latter approach and our ladder DSE result is more apparent as our result displays a much stronger Q^2-dependence. In particular, our result indicates a pole-like singularity for timelike Q^2, which can be attributed to the presence of a vector meson pole in the dressed quark-photon vertex. This singularity is evident in both the GIA and our full calculation, but not in the calculation using the BC ansatz. Again, the GIA does not reproduce the anomaly prediction without the additional ladder diagrams of Fig. 2.

IV. COMPARISON TO MESON EXCHANGE MODELS

The ladder DSE result clearly indicates a pole-like singularity in the timelike Q^2 region, due to the presence of a vector meson pole in the dressed quark-photon vertex. In addition to this pole, there are pole-like singularities from intermediate meson exchanges in the s, t and u channels, similar to the scalar and vector meson exchange contributions in π-π scattering [16]. Here however, the scalar meson exchange contribution is forbidden by spin/parity conservation. Thus only vector meson intermediate states contribute to γ-3π processes.

A. Vector meson dominance

The effective vector meson dominance (VMD) Lagrangian is

$$\mathcal{L}_{\rm int} = g_{\rho\pi\pi}\vec{\rho}_\mu \cdot \vec{\pi} \times \nabla^\mu \vec{\pi} + g_{\omega\rho\pi}\epsilon^{\mu\nu\lambda\sigma}\nabla_\mu \omega_\nu \nabla_\lambda \vec{\rho}_\sigma \cdot \vec{\pi} + e\left(\frac{m_\rho^2}{g_\rho}\rho_\mu^0 + \frac{m_\omega^2}{g_\omega}\omega_\mu\right)A^\mu, \quad (18)$$

where $\vec{\pi}, \vec{\rho}_\sigma, \omega_\nu$ and A^μ are the π, ρ, ω and photon fields, m_ω, m_ρ are the ω, ρ masses and $g_{\omega\rho\pi}$, $g_{\rho\pi\pi}$ are the $\omega \to \rho\pi$, $\rho \to \pi\pi$ coupling constants respectively. With this Lagrangian the VMD form factor for $\gamma \to \omega \to \rho\pi \to 3\pi$, is [35]

$$F^{3\pi}_{VMD}(s,t,u) = \frac{2em_\omega^2}{g_\omega}\frac{g_{\omega\rho\pi}g_{\rho\pi\pi}}{Q^2+m_\omega^2} \times \left(\frac{1}{m_\rho^2 - s} + \frac{1}{m_\rho^2 - t} + \frac{1}{m_\rho^2 - u}\right). \quad (19)$$

Note that this VMD form factor has vector meson poles in both the photon momentum Q^2 and the Mandelstam variables s, t and u. The pole in Q^2 is associated with an intermediate ω meson, whereas the poles in s, t and u are associated with ρ intermediate states.

The measured $\omega, \rho \to e^+e^-$ decay widths

$$\Gamma^\omega_{ee} = \frac{4\pi\alpha^2 m_\omega}{3g_\omega^2} = 0.60 \ \text{keV}, \quad (20)$$

$$\Gamma^\rho_{ee} = \frac{4\pi\alpha^2 m_\rho}{3g_\rho^2} = 6.85 \ \text{keV}, \quad (21)$$

determine the ω-photon, $g_\omega = 17.06$, and ρ-photon, $g_\rho = 5.01$, couplings which compare reasonably with the model calculations of 15.2 and 5.07, respectively [29] (see also Table I). The hadronic coupling, $g_{\rho\pi\pi}$, was previously predicted [32] in this model to be 5.14 which agrees favorably with the experimentally extracted value of 6.02.

Due to limited phase space, the $\omega \to \rho\pi$ decay is forbidden, precluding direct determination of $g_{\omega\rho\pi}$. However, this coupling can be related to the $\omega \to \pi^0\gamma$ decay, again using VMD for $\omega \to \pi^0\rho^0 \to \pi^0\gamma$

$$\Gamma^\omega_{\pi\gamma} = \frac{\alpha g_{\omega\rho\pi}^2 (m_\omega^2 - m_\pi^2)^3}{24 g_\rho^2 m_\omega^3}. \quad (22)$$

Using the measured width, $\Gamma^\omega_{\pi\gamma} = .734$ MeV, yields $g_{\omega\rho\pi} = 11.8$ GeV^{-1}. With these parameters the VMD prediction for the $\pi^0 \to \gamma\gamma$ anomaly, via $\pi^0 \to \omega\rho \to \gamma\gamma$, is

$$F^{2\gamma}_{VMD}(0) = \frac{8\pi\alpha g_{\omega\rho\pi}}{g_\rho g_\omega} = 0.0253 \ \text{GeV}^{-1}. \quad (23)$$

This is in excellent agreement with both the low-energy theorem, $F^{2\gamma}(0) = \alpha/(\pi f_\pi) = 0.0251$ GeV^{-1}, and the experimental value, 0.025 ± 0.001 GeV^{-1}.

Returning to the $F^{3\pi}(s,t,u)$ form factor, the VMD prediction in the chiral and zero momenta limits is

$$F^{3\pi}_{VMD}(0,0,0) = \frac{6e g_{\omega\rho\pi} g_{\rho\pi\pi}}{g_\omega m_\rho^2} = 12.6 \ \text{GeV}^{-3}. \quad (24)$$

This is above the low-energy theorem result, Eq. (11), but in potentially better agreement with the observed value, $12.9 \pm 0.9 \pm 0.5$ GeV^{-3}, measured at higher energy (note that Ref. [36] quotes a corrected experimental value of 11.9 GeV^{-3}). By reducing $g_{\rho\pi\pi}$ it is possible for the VMD

form factor to agree with the low-energy theorem, however this conflicts with the KSRF relation [37,38]

$$g_{\rho\pi\pi}=m_\rho/(\sqrt{2}f_\pi). \tag{25}$$

Further, the VMD result is not consistent with anomalous Ward identities of Ref. [5]. These two issues can be resolved by adding a contact term to the Lagrangian

$$\mathcal{L}_{\text{contact}}=G_\omega\epsilon^{\mu\nu\lambda\sigma}\omega_\mu\nabla_\nu\vec{\pi}\cdot\nabla_\lambda\vec{\pi}\times\nabla_\sigma\vec{\pi}, \tag{26}$$

with the coupling G_ω governing the direct $\omega\to 3\pi$ decay. This gives the modified VMD result [39,40]

$$\tilde{F}^{3\pi}_{VMD}(s,t,u)=\frac{-6em_\omega^2}{g_\omega}\frac{G_\omega}{Q^2+m_\omega^2}+F^{3\pi}_{VMD}(s,t,u). \tag{27}$$

References [39,40] determine G_ω by satisfying both Eq. (25) and the low-energy theorem for γ-3π. Further, these analyses also invoke SU(2) flavor symmetry and universality using the relations $g_\omega=3g_\rho=3g_{\rho\pi\pi}$, which are reasonable, to obtain

$$G_\omega=\frac{g_{\rho\pi\pi}}{16\pi^2\ f_\pi^3}. \tag{28}$$

With these relations the modified form factor can be more succinctly expressed in terms of only f_π, using Eq. (17), instead of meson coupling constants

$$\tilde{F}^{3\pi}_{VMD}(s,t,u)=-\frac{1}{2}\frac{m_\omega^2F^{3\pi}_{\text{anomaly}}(0,0,0)}{Q^2+m_\omega^2}\times\left[1-\left(\frac{m_\rho^2}{m_\rho^2-s}+\frac{m_\rho^2}{m_\rho^2-t}+\frac{m_\rho^2}{m_\rho^2-u}\right)\right]. \tag{29}$$

B. Comparison of DSE and VMD for $\gamma\to 3\pi$

Because of the established phenomenological success of VMD, it is worthwhile to compare the two VMD form factors to our DSE result. In particular, it is of interest to ascertain that the DSE approach can reproduce the resonance features of the VMD. In doing so, consistency mandates that the VMD phenomenological parameters be replaced by the corresponding values calculated in the DSE model. All necessary DSE coupling constants, except for $g_{\omega\rho\pi}$ which is discussed below, are listed in Table I.

In Fig. 5 the pure, Eq. (19), and modified, Eq. (29), VMD form factors are compared to the DSE result from $Q^2\approx 0$ to the ω resonance region. The ladder DSE and VMD results are in good qualitative agreement. In particular, the ω resonance exhibited in the VMD is well reproduced by the ladder DSE approach. Note that the DSE approach naturally agrees with the low-energy theorem while only by construction can the modified VMD form factor reproduce this result; the pure VMD form factor does not reproduce the correct low-energy limit.

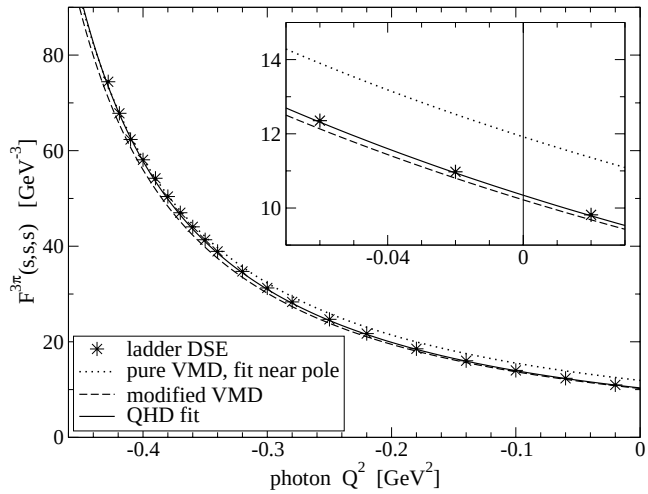

FIG. 5. Comparison of the ladder DSE calculation (asterisk) to the DSE parametrized pure (dotted) and modified (dashed) VMD form factors, $F^{3\pi}(s,s,s)$, as a function of Q^2. The solid curve represents a phenomenological QHD fit to the DSE form factor.

Because of off-shell ambiguities, one cannot consistently calculate the unphysical $\omega\rho\pi$ amplitude. However, by fitting the pure VMD form factor, Eq. (19), to the DSE result near the ω pole and using the calculated values of Table I for the remaining coupling constants in that equation, we extract the value $g_{\omega\rho\pi}=10.3$ GeV^{-1}. This is slightly below the phenomenological VMD result of 11.8 GeV^{-1} but significantly lower than other theoretical values: SU(3) flavor symmetry, 16 GeV^{-1} [41]; QCD sum rules, 15 to 17 GeV^{-1} [42]; light-cone sum rules, 16 GeV^{-1} [43].

In addition, Fig. 5 also displays a form factor based on a purely phenomenological quark-hadron model (QHD) incorporating both contact interactions and meson-exchange contributions

$$F^{3\pi}_{QHD}(s,t,u)=C_{\gamma 3\pi}-\frac{6m_\omega^2C_{\omega 3\pi}}{g_\omega(Q^2+m_\omega^2)}-C_{\gamma\pi\rho}\left(\frac{m_\rho^2g_{\rho\pi\pi}}{m_\rho^2-s}+\frac{m_\rho^2g_{\rho\pi\pi}}{m_\rho^2-t}+\frac{m_\rho^2g_{\rho\pi\pi}}{m_\rho^2-u}\right)+F^{3\pi}_{VMD}(s,t,u). \tag{30}$$

The three coefficients C are determined by fitting the ladder DSE calculation at different s, t, u and Q^2 values. An accurate fit over a large kinematical range is obtained with $C_{\gamma 3\pi}=0.248$ GeV^{-3}, $C_{\omega 3\pi}=5.94$ GeV^{-3} and $C_{\gamma\pi\rho}=0.028$ GeV^{-3}. This provides a useful analytic representation of the DSE form factor.

C. Comparison of DSE and VMD for $\gamma\pi\to\pi\pi$

Finally, we consider the process $\gamma\pi\to\pi\pi$. It is described by the same form factor $F^{3\pi}(s,t,u)$ as the process $\gamma\to 3\pi$, but the kinematical variables are different. In general, $s\neq t$

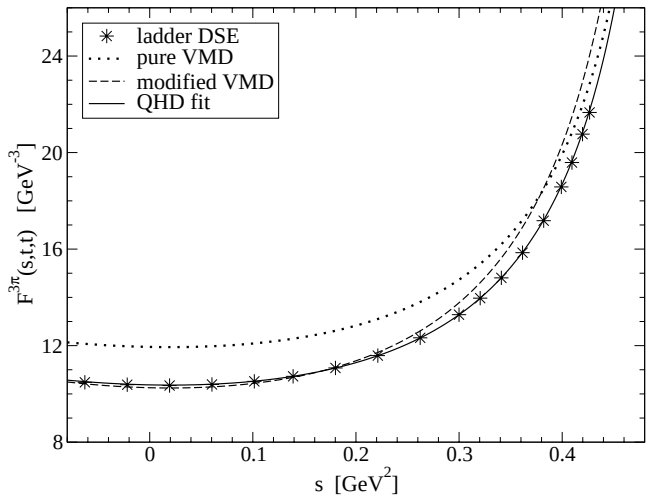

FIG. 6. Comparison of the ladder DSE (asterisk), pure VMD (dotted), modified VMD (dashed) and fitted QHD (solid) form factors, $F^{3\pi}(s,t,t)$, as a function of s at $Q^2=0$.

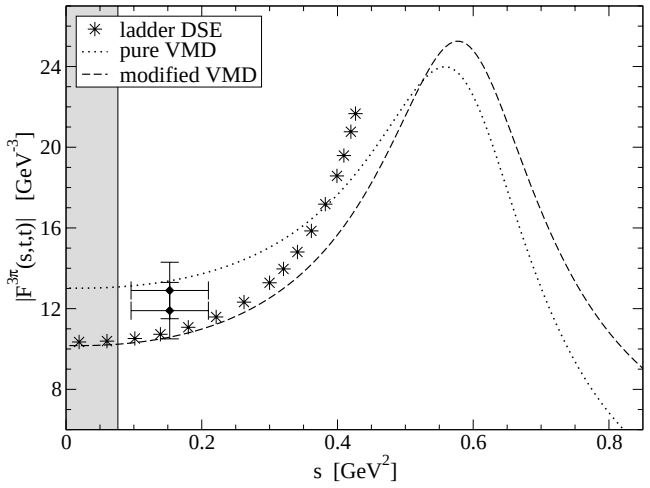

FIG. 7. Comparison of DSE (asterisk), pure VMD (dotted), and modified VMD (dashed) form factors, $F^{3\pi}(s,t,t)$, with data at $Q^2=0$. The experimental coupling constants, masses and width are used in both VMD form factors (the shaded region is unphysical). The data point is from Ref. [6] (reanalyzed in Ref. [36]); new experimental results from JLab are anticipated [11] in the region $0.27\ \text{GeV}^2<s<0.72\ \text{GeV}^2$.

$\neq u$, but for simplicity, we only consider the more symmetric case $t=u$. The kinematically allowed region is $s>4m_\pi^2$ and $t,u<0$.

In Fig. 6 we compare our DSE results with the VMD and phenomenological meson exchange form factors. For fixed $Q^2=0$, the ω meson does not appear as a pole in the form factor. The ρ pole in the s channel on the other hand is clearly identifiable. In addition, there are also poles in the unphysical region, corresponding to intermediate ρ mesons in the t- and u-channels.

With the same parameters as in the previous subsection, the pure VMD form factor agrees very well with the ladder DSE calculation near the ρ pole, but overestimates the form factor by about 15% near threshold. The modified VMD form factor on the other hand agrees very well with the DSE result near threshold, but starts to deviate for increasing values of s. The purely phenomenological QHD form factor can describe the DSE form factor accurately both near threshold and in the resonance region, not only at $Q^2=0$ but also at other values of Q^2. However, this is not surprising, since it was fitted to our DSE result to provide an analytic representation of our results.

V. COMPARISON WITH EXPERIMENTAL DATA

Finally, for the benefit of experimentalists the same three form factors are compared to the limited data. We use the phenomenological parameters in the VMD form factors permitting their most favorable prediction. In particular, the ρ mass in Eqs. (19) and (29) is replaced by $m_\rho-(i/2)\Gamma_\rho$ where $\Gamma_\rho=149$ MeV is the experimental width of the ρ meson. This changes the ρ-meson pole singularity in Fig. 6 to a resonance peak with a finite maximum. We ignore the much smaller ω width since we consider the process $\gamma\pi\to\pi\pi$ for on-shell photons ($Q^2=0$) only.

The ladder truncation of the inhomogeneous BSE Eq. (12), on the other hand, has a real pole singularity at the ρ-mass. One would need to include two-pion intermediate stated in the interaction kernel to consistently produce a ρ-meson width.

In Fig. 7 we display the absolute value of both the pure and the modified VMD form factors as functions of s, the total energy of the two outgoing pions, for $t=u=(3m_\pi^2-s)/2$ and on-shell photons. For comparison, we also show the ladder DSE calculation below the ρ-pole singularity. The modified VMD form factor appears to be the most realistic and agrees quite well with the microscopic DSE calculation near threshold, $s=4m_\pi^2$. At larger values of s it reflects the ρ-meson width and therefore exhibits a resonance peak rather than the pole singularity of the ladder DSE calculation. The large error bar on the experimental data point precludes definitive conclusions but new, more precise measurements are in progress which should provide useful insight and model constraints.

VI. CONCLUSION

In summary, the anomalous form factor for γ-3π processes has been calculated in a self-consistent Dyson-Schwinger, Bethe-Salpeter formulation in the rainbow-ladder truncation. The significant finding is that to reproduce the fundamental low-energy theorem, it is necessary to go beyond the generalized impulse approximation. Specifically, one has to include complete sets of ladder diagrams in the s, t and u channels.

The ladder DSE result is in good agreement with vector meson dominance. The ladder dressing of the quark-photon vertex is essential for generating the ω resonance in the process $\gamma\to\omega\to3\pi$. Inclusion of the ladder diagrams beyond the GIA (see Fig. 2) is necessary to produce an intermediate ρ-meson state in the two-pion channel. A meson-exchange form factor incorporating both contact interactions and meson-exchange contributions, fitted to our DSE calculation,

provides a useful analytic representation of our results over a large kinematical range.

Our predictions are also in agreement with the limited data near threshold and await confrontation with additional and more precise measurements currently in progress. For larger values of s we expect the modified VMD form factor to be in better agreement with experiment since it includes the ρ-meson width. These results should also be of interest to experimentalists investigating double pion photoproduction.

Future work will address calculating the width for $\omega \to 3\pi$ as well as the strangeness processes $\gamma \to K\bar{K}\pi$ and $\gamma K \to \pi K$. Longer term, this framework will be extended to describe meson electroproduction from a nucleon target.

ACKNOWLEDGMENTS

This work was supported by the Department of Energy under grant DE-FG02-97ER41048. Calculations were performed with resources provided by the National Energy Research Scientific Computing Center and the North Carolina Supercomputer Center.

[1] S.L. Adler, Phys. Rev. **177**, 2426 (1969).
[2] J.S. Bell and R. Jackiw, Nuovo Cimento A **60**, 47 (1969).
[3] S.L. Adler, B.W. Lee, S.B. Treiman, and A. Zee, Phys. Rev. D **4**, 3497 (1971).
[4] M.V. Terent'ev, Phys. Lett. **38B**, 419 (1972).
[5] R. Aviv and A. Zee, Phys. Rev. D **5**, 2372 (1972).
[6] Y.M. Antipov *et al.*, Phys. Rev. D **36**, 21 (1987).
[7] S.I. Dolinsky *et al.*, Phys. Rep. **202**, 99 (1991).
[8] DM2 Collaboration, A. Antonelli *et al.*, Z. Phys. C **56**, 15 (1992).
[9] L.M. Barkov *et al.*, JETP Lett. **46**, 164 (1987).
[10] R.A. Miskimen, K. Wang, and A. Yagneswaran, Study of the Axial Anomaly using the $\gamma\pi^+ \to \pi^+\pi^0$ Reaction Near Threshold, Jefferson Lab Experiment 94-015, 1994.
[11] R.A. Miskimen (private communication).
[12] R. Alkofer and C.D. Roberts, Phys. Lett. B **369**, 101 (1996).
[13] B. Bistrovic and D. Klabucar, Phys. Lett. B **478**, 127 (2000).
[14] B. Bistrovic and D. Klabucar, Phys. Rev. D **61**, 033006 (2000).
[15] P. Bicudo, S.R. Cotanch, F.J. Llanes-Estrada, P. Maris, E. Ribeiro, and A. Szczepaniak, Phys. Rev. D **65**, 076008 (2002).
[16] S.R. Cotanch and P. Maris, Phys. Rev. D **66**, 116010 (2002).
[17] C.D. Roberts and A.G. Williams, Prog. Part. Nucl. Phys. **33**, 477 (1994).
[18] C.D. Roberts and S.M. Schmidt, Prog. Part. Nucl. Phys. **45**, S1 (2000).
[19] R. Alkofer and L. von Smekal, Phys. Rep. **353**, 281 (2001).
[20] P. Maris and C.D. Roberts, Int. J. Mod. Phys. E **15**, 297 (2003).
[21] C.H. Llewellyn-Smith, Ann. Phys. (N.Y.) **53**, 521 (1969).
[22] P. Maris and C.D. Roberts, Phys. Rev. C **56**, 3369 (1997).
[23] R. Delbourgo and M.D. Scadron, J. Phys. G **5**, 1631 (1979).
[24] A. Bender, C.D. Roberts, and L. Von Smekal, Phys. Lett. B **380**, 7 (1996).
[25] P. Maris, C.D. Roberts, and P.C. Tandy, Phys. Lett. B **420**, 267 (1998).
[26] C.D. Roberts, Nucl. Phys. **A605**, 475 (1996).
[27] P. Maris and P.C. Tandy, Phys. Rev. C **62**, 055204 (2000).
[28] J.S. Ball and T.-W. Chiu, Phys. Rev. D **22**, 2542 (1980).
[29] P. Maris and P.C. Tandy, Phys. Rev. C **60**, 055214 (1999).
[30] The Jefferson Lab F_π Collaboration, J. Volmer *et al.*, Phys. Rev. Lett. **86**, 1713 (2001).
[31] P. Maris and P.C. Tandy, Phys. Rev. C **65**, 045211 (2002).
[32] D. Jarecke, P. Maris, and P.C. Tandy, Phys. Rev. C **67**, 035202 (2003).
[33] P. Maris, C.D. Roberts, S.M. Schmidt, and P.C. Tandy, Phys. Rev. C **63**, 025202 (2001).
[34] Particle Data Group, D.E. Groom *et al.*, Eur. Phys. J. C **15**, 1 (2000).
[35] S. Rudaz, Phys. Rev. D **10**, 3857 (1974).
[36] B.R. Holstein, Phys. Rev. D **53**, 4099 (1996).
[37] K. Kawarabayashi and M. Suzuki, Phys. Rev. Lett. **16**, 255 (1966).
[38] Riazuddin and Fayyazuddin, Phys. Rev. **147**, 1071 (1966).
[39] S. Rudaz, Phys. Lett. **145B**, 281 (1984).
[40] T.D. Cohen, Phys. Lett. B **233**, 467 (1989).
[41] P. Rotelli and M.D. Scadron, Nuovo Cimento Soc. Ital. Fis., A **15**, 643 (1973).
[42] V.L. Eletsky, B.L. Ioffe, and Y.I. Kogan, Phys. Lett. **122B**, 423 (1983).
[43] M. Lublinsky, Phys. Rev. D **55**, 249 (1997).